https://dx.doi.org/10.1016/j.compscitech.2021.109079



# Understanding the Sensitivity of Thin-Film Graphene/Polymer Nanocomposite Strain Sensors to Ultrasonic Waves: Analytical and Experimental Analysis

Ruiqi Guan[a,b], Fangxin Zou[a,*], Dan Li[c], Wenming Liu[d], Congping Wu[d]

[a] Department of Aeronautical and Aviation Engineering, The Hong Kong Polytechnic University, Hung Hom, Kowloon, Hong Kong SAR, China

[b] College of Civil Engineering, Huaqiao University, Xiamen, Fujian 361021, China

[c] Technology and Engineering Center for Space Utilization, Chinese Academy of Sciences, Beijing, China

[d] Kunshan Innovation Institute of Nanjing University, Jiangsu Key Laboratory for Nano Technology, Nanjing University, Nanjing, Jiangsu, China

## Abstract

Thin-film graphene/polymer nanocomposite sensors have been shown to be exceptionally sensitive to ultrasonic waves, making them promising next-generation candidates for structural integrity monitoring. However, the ultrasonic sensing mechanism of these sensors has never been scrutinized, restricting the deployment of these sensors to real-life applications. Herein, we carry out the first-ever study on the ultrasonic sensing mechanism of thin-film graphene/polymer nanocomposite sensors, through complementary physical experiments and analytical modelling. At first, sensors were precisely fabricated from nanofillers of different

* Corresponding author. Email: frank.zou@polyu.edu.hk

sizes and different matrix materials, and their electrical conductivities and ultrasonic sensitivities were measured. Analytical models that are based on the effective medium theory and the various contact modes between graphene nanofillers, entailing interphase regions and the quantum tunneling effect, were then established and fitted to the experimental results to reveal a series of microscopic characteristics of the sensors fabricated. Through a systematic analysis, it was found that the sizes of nanofillers and the properties of matrices significantly influence the microscopic morphologies and strain-induced dynamics of the sensors, in turn dictating their electrical conductivities and ultrasonic sensitivities. This insightful study will serve as the foundation for realizing applications of high-sensitivity thin-film graphene/polymer nanocomposite sensors in real-life ultrasound-based structural integrity monitoring scenarios.

**Keywords:** A. nano composites, B. sensing, C. material modelling, C. multi-mechanism modelling, D. ultrasonic testing.

## 1. Introduction

Graphene/polymer nanocomposites have attracted much attention due to their exceptional mechanical, electrical and thermal properties. They are also potential replacements for conventional strain sensors owing to their physical flexibilities and high sensitivities. Recently, it has been found that thin-film graphene/polymer nanocomposite strain sensors possess an outstanding sensitivity to dynamic strains and can be well utilized for *in situ* structural integrity monitoring through acquiring ultrasonic wave-induced high-frequency microscopic vibrations [1-3]. However, no work has been done, to the best of the authors' knowledge, to understand

the underlying ultrasonic sensing mechanism of these sensors, challenging the future development of these sensors into mature technologies.

To understand the sensing mechanism of a nanocomposite strain sensor, the electrical conductivity and the percolation threshold of the sensor need to be determined at first, since they are the key parameters that reflect the sensor's performance. Percolation thresholds are usually estimated by the classical percolation theory [4] through evaluating electrical conductivities by the power-law model [5, 6]. While the model provides a simple approach for fitting experiment data, it does not interpret the relationship between the electrical conductivity of a sensor and the nanofillers, the matrix, or the interphase regions (the regions between the nanofillers and the matrix) in the sensor. In fact, the electrical conductivities and the percolation thresholds of graphene/polymer nanocomposite strain sensors have been found to be highly dependent on the orientations and the aspect ratios of nanofillers and the properties of matrices [7-10], which collectively dictate the properties of interphase regions and the quantum tunneling effect. The influence of these parameters on sensitivities would be more pronounced for strain sensors used for acquiring ultrasonic waves, since these sensors essentially respond to high-frequency micro-vibrations on the basis of the quantum tunneling effect [11]. Numerous analytical studies have been conducted to evaluate the sensitivities of nanocomposite strain sensors. An analytical model [12] that entails the properties of nanofillers and matrices was developed to predict the electrical conductivities of nanocomposites. However, interphase regions and the quantum tunneling effect are not considered in this model. Hashemi et al. [13] constructed a continuum model for graphene/polymer nanocomposites that

includes the influence of interphase regions and the quantum tunneling effect on electrical conductivities. Nevertheless, the model fails to embrace nanofiller shape as a key parameter for the prediction of percolation thresholds. Mazaheri et al. [7] also took into account interphase regions in their theoretical model for the electrical conductivities of graphene/polymer nanocomposites. They modelled each nanofiller as a graphene particle coated with a thin layer of matrix material and obtained results that match well with previous experimental data. Furthermore, Wang et al. [8] and Xia et al. [14] came up with theoretical models for both the electrical conductivities and the dielectric permittivity of graphene/polymer nanocomposites. In their models, the effects of interphase regions, quantum tunneling and other more complex features, such as the orientations and the agglomeration of nanofillers, are well taken into account.

The micro-scale or even nano-scale vibrations induced by ultrasonic waves at 10s kHz to a few MHz are distinct from the large quasi-static strains induced by tensile or compressive loads. The major sensing mechanism of graphene/polymer nanocomposites for microscopic strains under 0.3% is believed to be the quantum tunneling effect [11], which induces changes in the tunneling resistances between adjacent nanofillers. An analytical model [15] was established to explain the different sensitivities or gauge factors (GFs) exhibited by graphene/polymer nanocomposites under tension and flexure, through considering two types of contact modes between nanofillers. The aforementioned model was, in fact, inspired by an earlier model of carbon nanotubes/polymer nanocomposites [16]. Nevertheless, both models are for large quasi-static strains and do not suit the micro-vibrations in the ultrasonic regime.

Also, interphase regions and tunneling barriers, which would influence sensitivities at microscopic strain levels [17, 18], are not entailed in these models. Therefore, to determine the sensitivities of nanocomposite strain sensors to ultrasonic waves and to analyze their ultrasonic sensing mechanism, a novel approach has to be derived and adopted.

In this work, the ultrasonic sensing mechanism of thin-film graphene/polymer nanocomposite strain sensors will be explored for the first time. Sensors that are made from nanofillers of different sizes and different types of matrix materials were precisely fabricated by spray coating. The responses of the sensors to ultrasonic waves were acquired experimentally. The sensitivities of the sensors were then evaluated. Comprehensive analytical models for the electrical conductivities and the sensitivities of the sensors, which include not only the properties of the constituent materials, but also interphase regions and the quantum tunneling effect, were established. The models were fitted to the experimental results in order to carry out an in-depth, rigorous investigation on how the sizes of nanofillers and the properties of matrices would affect the microscopic morphologies and strain-induced dynamics of the sensors and, in turn, determine their sensitivities to ultrasonic waves. This work significantly enhances the current understanding of the behavior of thin-film graphene/polymer nanocomposite strain sensors in the ultrasonic regime, potentially allowing these sensors to be deployed to real-world applications of *in situ* structural integrity monitoring.

## 2. Experimental

### 2.1.Materials

Three types of graphene nanofillers, each with a distinct dimension, were purchased from

Shanghai Aladdin Biochemical Technology Co., China. Three types of matrix materials were procured: (i) polyvinylpyrrolidone (PVP; K30, Shanghai Macklin Biochemical Co., China), (ii) polyvinylidene fluoride (PVDF; Kynar HSV 900, Arkema, France), and (iii) polyvinyl alcohol (PVA; Type 105, Shanghai Macklin Biochemical Co., China). The graphene nanofillers and the matrix materials were made into spraying inks with either distilled water or dimethylformamide (DMF; 99.8%, Sigma-Aldrich, USA) for the fabrication of nanocomposite sensors.

### 2.2.Spray coating of nanocomposite strain sensors

Owing to its proven capability of fabricating highly reproducible thin-film nanocomposite strain sensors [19], ultrasonic atomization-assisted spray coating was adopted to fabricate the nanocomposite sensors concerned in this work. Two groups of spraying inks were prepared. While the inks in the first group differ in nanofiller size, those in the second group differ in matrix type. The detailed parameters of the spraying inks are given in Table 1. To ensure that the graphene nanofillers were uniformly dispersed, all the spraying inks were first mechanically stirred by a magnetic stirrer for 2 hours and then put into an ultrasonic bath for 12 hours. The sensors that were fabricated from these inks were labeled as [G1, G2, G3] and [M1, M2, M3].

**Table 1.** Details of the spraying inks.

| Group No. | Graphene dimension | | Matrix | Solvent | Graphene content | Label |
|---|---|---|---|---|---|---|
| | **Diameter (μm)** | **Thickness (nm)** | | | | |
| **1** | 6 | 7 | PVP | Distilled water | 4-15 vol% | G1 |
| | 6 | 3.47 | | | | G2 |

| | | | | | | |
|---|---|---|---|---|---|---|
| | 3 | 3.47 | | | | G3 |
| **2** | 6 | 7 | PVP | Distilled water | 5.5-15 vol% | M1 |
| | | | PVA | | | M2 |
| | | | PVDF | DMF | | M3 |

20 mm × 15 mm nanocomposite sensors were fabricated using a commercial ultrasonic atomization-assisted spray coating system (Sunlaite SP202, Jiangsu Yanchang Sunlaite New Energy Co., China). Through ultrasonic sensing experiments, the optimal number of spraying layers for the nanocomposite sensors concerned in this work was found to be 10. The fabrication process of the sensors, the setup for the ultrasonic experiments, and the process of determining the optimal number of spraying layers are all detailed in the Supplementary Information.

## 3. Results and discussion

### 3.1.Morphologies of nanocomposite sensors

The surface morphologies of the nanocomposite sensors were characterized by scanning electron microscopy (SEM; see the Supplementary Information for the method). From the results shown in Figure 1(a)-(e), it is observed that graphene nanofillers were well dispersed in the three types of matrix materials used, indicating the high quality of the spray-coated thin-film nanocomposite sensors. SEM was also used to double-check the information provided by the supplier on the average diameters of the three types of graphene nanofillers. As shown in Figure 1(a)-(c), the diameters of the graphene nanofillers in the G1 and the G2 sensor are indeed around 6 μm, while the diameters of the nanofillers in the G3 sensor are much smaller and

close to 3 μm.

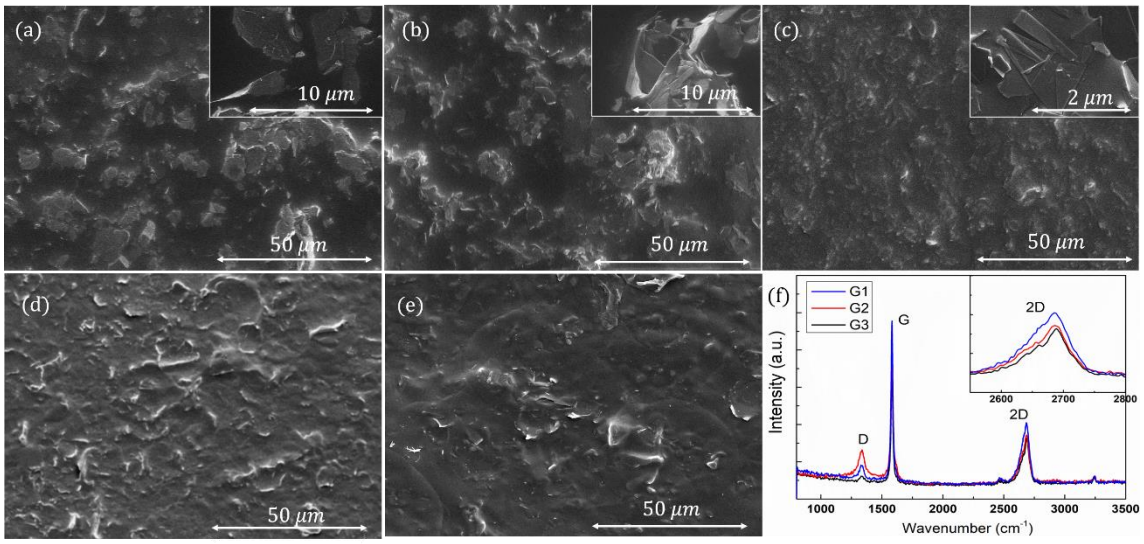


**Figure 1.** Surface morphologies of nanocomposite sensors (graphene content: 8.5 vol%): (a) G1/M1 (nanofiller diameter: 6 μm), (b) G2 (nanofiller diameter: 6 μm), (c) G3 (nanofiller diameter: 3 μm), (d) M3 and (e) M2. (f) Raman spectra of the graphene nanofillers in the G1 sensor (nanofiller thickness: 7 nm), the G2 sensor (nanofiller thickness: 3.47 nm) and the G3 sensor (nanofiller thickness: 3.47 nm).

The thicknesses of the graphene nanofillers in the nanocomposite sensors were examined through Raman spectroscopy (see the Supplementary Information for the method). The Raman spectra of the G1, the G2 and the G3 sensor, shown in Figure 1(f), all present a D band, a G band and a 2D band. For the three sensors concerned, the 2D band appeared to be the most significant indicator for the thicknesses of graphene nanofillers. The existence of multi-layer graphene nanofillers in each of the sensors led to the overlapping of several modes in the 2D band, as opposed to a single symmetric 2D peak. The 2D bands of the G2 and the G3 sensor, which are made from graphene nanofillers of the same thickness, are very similar. In contrast, the G1 sensor, which contains thicker graphene nanofillers, would have given rise to more overlapping modes in the 2D band and, hence, presents a drastically different 2D band in both shape and position.

### 3.2.Responses of nanocomposite sensors to ultrasonic waves

The ultrasonic signals that were acquired by a set of nanocomposite sensors are displayed in Figure 2. The group velocities of the $S_0$ and the $A_0$ modes acquired by these sensors are close to the theoretical values of 3280 m/s and 1990 m/s (see the Supplementary Information for the calculation of the theoretical values), meaning that the sensors did not exhibit any delay in responding to the high-frequency micro-vibrations induced by ultrasonic waves. A number of observations can be made from the experimental results. First of all, the G1 sensor possesses a much higher sensitivity than the G2 and the G3 sensors, as seen in Figure 2(a). Also, the $A_0$ modes acquired by the G2 and the G3 sensors are too marginal compared to the $S_0$ modes. Furthermore, as shown in Figure 2(b), the M2 sensor possesses the highest sensitivity in Group 2, followed by the M1 sensor, whereas the sensitivity of the M3 sensor is significantly lower. Based on these observations, it is clear that the sensitivities of thin-film graphene/polymer nanocomposite sensors are highly dependent on the sizes of nanofillers and the properties of matrices. Therefore, it is necessary to look into the ultrasonic sensing mechanism of these sensors to understand how their sensitivities are influenced by these key parameters.

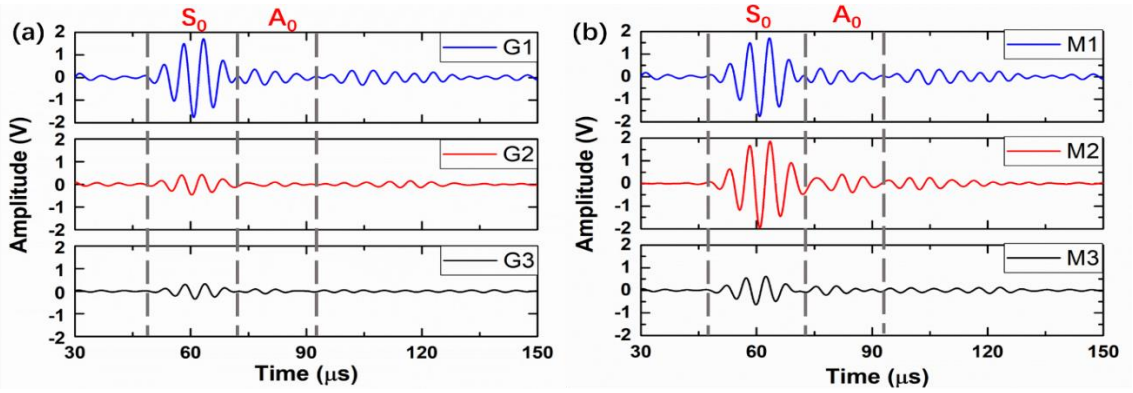


**Figure 2.** Ultrasonic signals acquired by (a) Group 1 and (b) Group 2 nanocomposite sensors (graphene content: 8.5 vol%). The dash lines indicate the arrival times and the durations of the $S_0$ and the $A_0$ modes.

### 3.3. Analytical model for electrical conductivities and tunneling resistances of thin-film graphene/polymer nanocomposite sensors

#### 3.3.1. Electrical conductivities of coated graphene nanofillers

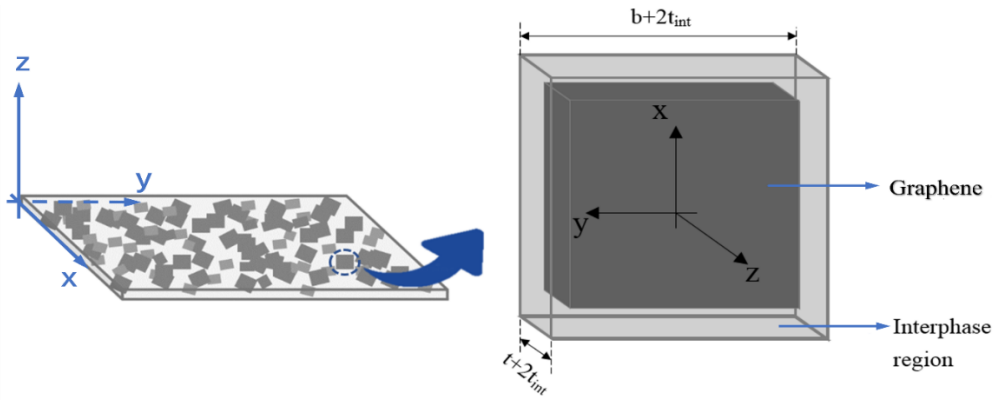


**Figure 3.** Model of a thin-film graphene/polymer nanocomposite sensor with coated nanofillers that are highly aligned in the x-y plane.

As illustrated in Figure 3, the model of a square-shape graphene nanofiller coated by a thin layer of matrix material, known as the interphase region, is established. The embedded graphene nanofiller measures $b \times b \times t$ and the surrounding interphase region has a thickness of $t_{int}$. Since the model is symmetric in the x-y plane, the transverse electrical conductivities of the coated graphene nanofiller in the x-direction ($\sigma_1$) and in the y-direction ($\sigma_2$) are the same. The transverse and the longitudinal electrical conductivities ($\sigma_3$) of the coated nanofiller can be calculated by [7, 20]

$$\sigma_1 = \sigma_2 = \frac{\sigma_{int}(t+2t_{int})\{\sigma_g bt + \sigma_{int}[(b+2t_{int})(t+2t_{int}) - bt]\}}{2t_{int}\{\sigma_g bt + \sigma_{int}[(b+2t_{int})(t+2t_{int}) - bt]\}}, \quad (1)$$

$$\sigma_3 = \frac{\sigma_{int}(t+2t_{int})\left[\sigma_g b^2 + \sigma_{int}(4bt_{int} + 4{t_{int}}^2)\right]}{2t_{int}\sigma_g b^2 + 2t_{int}\sigma_{int}(4bt_{int} + 4{t_{int}}^2) + \sigma_{int} b(b+2t_{int})^2}, \quad (2)$$

where $\sigma_g$ and $\sigma_{int}$ are the electrical conductivities of the embedded graphene nanofiller and

the interphase region, respectively.

As the volume fraction of the graphene nanofillers in a nanocomposite sensor increases, the occurrence of quantum tunneling inside the sensor becomes more probable, since the distances between adjacent nanofillers become smaller and, hence, the tendency for electrons to move between nanofillers is enhanced. Consequently, the electrical conductivity of the interphase regions around the nanofillers also increases. This increase in electrical conductivity is most significant at the percolation threshold of the sensor. To entail the quantum tunneling effect in the model for the electrical conductivity of an interphase region, the Cauchy's statistical function is used [8, 21]. Therefore, the tunneling-assisted electrical conductivity of an interphase region can be written as

$$\sigma_{int} = \frac{\sigma_{int,0}}{\tau(c_1, c_1^*(\varphi), \gamma)}, \tag{3}$$

where

$$\tau(c_1, c_1^*(\varphi), \gamma) = \frac{F(1, c_1^*(\varphi), \gamma) - F(c_1, c_1^*(\varphi), \gamma)}{F(1, c_1^*(\varphi), \gamma) - F(0, c_1^*(\varphi), \gamma)}, \tag{4}$$

in which

$$F(c_1, c_1^*(\varphi), \gamma) = \frac{1}{\pi} arctan\left(\frac{c_1 - c_1^*(\varphi)}{\gamma}\right) + \frac{1}{2}. \tag{5}$$

In Equations (3), (4) and (5), $\sigma_{int,0}$ is the intrinsic electrical conductivity of the interphase region, related to the electrical conductivity of the matrix coating and the bonding quality between the embedded graphene nanofiller and the matrix coating [14], i.e., the imperfection level of the interphase region. $c_1$ is the volume fraction of the graphene nanofillers in the sensor, $c_1^*(\varphi)$ is the volume fraction of the graphene nanofillers at the percolation threshold of the sensor, related to in-plane orientation ($\varphi$) of the nanofillers, and $\gamma$ is a scaling factor that

is linked to the trend of the function near the percolation threshold.

At volume fractions that are close to the percolation threshold, the graphene nanofillers in the nanocomposite sensors fabricated can be assumed as randomly distributed and oriented in the x-y plane, due to the use of spray coating. Therefore, $c_1^*(\varphi)$ can be simplified as [22]

$$c_1^*(\varphi) = \frac{2\pi b^2 t}{(2t_{int} + b)^3}. \quad (6)$$

### 3.3.2. Effective electrical conductivities of nanocomposite sensors

The effective medium theory is employed to derive the electrical conductivities of nanocomposite sensors with highly aligned graphene nanofillers. The nanocomposite sensors in this work are essentially thin films. Therefore, when they respond to ultrasonic waves, their in-plane electrical conductivities would play much more dominant roles than their out-of-plane counterparts. As a result, only the in-plane electrical conductivities of the sensors need to be taken into account, hereinafter simply referred to as the effective electrical conductivities of the sensors ($\sigma_e$). The effective electrical conductivity of a nanocomposite sensor with highly aligned graphene nanofillers can be solved by [14]

$$c_0 \frac{\sigma_e(\sigma_m - \sigma_e)}{\sigma_e + S_{11}^0(\sigma_m - \sigma_e)} + c_1 \frac{\sigma_e(\sigma_1 - \sigma_e)}{\sigma_e + S_{11}(\sigma_1 - \sigma_e)} = 0\,, \quad (7)$$

where $c_0 = 1 - c_1$ and $\sigma_m$ are the volume fraction and the electrical conductivity of the matrix, $S_{11} = \frac{\pi t}{4b}$ is a component of the Eshelby's S-tensor for the graphene nanofillers [14, 23], and $S_{11}^0 = \frac{1}{3}$ is a component of the Eshelby's S-tensor for the matrix [23-25].

The thickness and the intrinsic electrical conductivity of the interphase regions in a nanocomposite sensor can be estimated by fitting Equation (7) to the experimentally measured

electrical conductivities of the sensor at different graphene contents. By doing so, the influence of the sizes of nanofillers and the properties of matrices on the microscopic properties of the interphase regions in thin-film graphene/polymer nanocomposite sensors can be studied.

### 3.3.3. Tunneling resistances of nanocomposite sensors

To comprehensively characterize the mechanism of the tunneling resistance changes of thin-film graphene/polymer nanocomposite sensors when they respond to micro-vibrations induced by ultrasonic waves, an analytical model of the tunneling resistances of these sensors is established based on two different types of contact modes between graphene nanofillers [15], as illustrated in Figure 4. Interphase regions are also considered when calculating tunneling resistances.

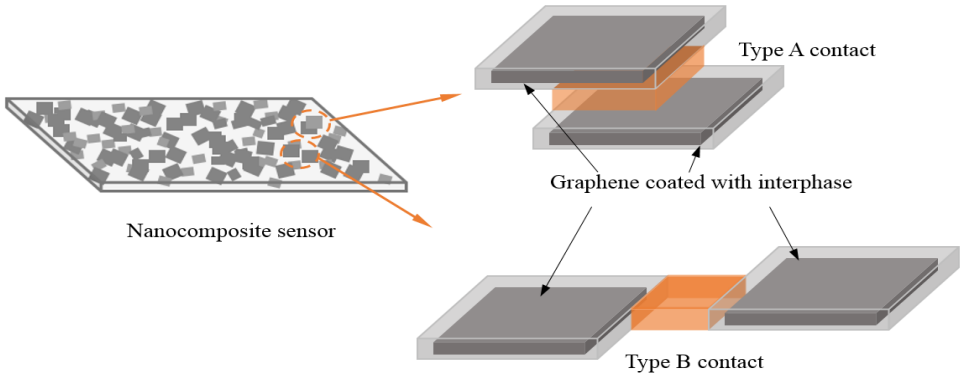


**Figure 4.** Schematics of the two types of contact modes between the graphene nanofillers in thin-film nanocomposite sensors.

In a Type A contact mode, quantum tunneling takes place within the out-of-plane overlap between two adjacent nanofillers. In Type B contact mode, quantum tunneling occurs between the ends of two adjacent nanofillers. The tunneling resistances of a Type A contact and a Type B contact can be described by the following expressions which are derived from the well-known Simmons' equation [18]

$$R_A = \frac{h^2 d_A}{S_A e^2 \sqrt{2m\lambda}} exp\left(\frac{4\pi d_A}{h}\sqrt{2m\lambda}\right), \tag{8}$$

$$R_B = \frac{h^2 d_B}{S_B e^2 \sqrt{2m\lambda}} exp\left(\frac{4\pi d_B}{h}\sqrt{2m\lambda}\right), \tag{9}$$

where $h$ is the Planck constant, $e$ and $m$ are the charge and the mass of an electron, $\lambda$ is tunneling barrier height of the matrix, $d_A$ and $d_B$ are the tunneling distances of the two contacts, and $S_A$ and $S_B$ are the contact areas.

The tunneling distances of the two contacts are related to the total strain experienced by the sensor ($\varepsilon$) by the Poisson's effect as

$$d_A = (1 - \nu\varepsilon)d_{A0}\,, \tag{10}$$

$$d_B = (1 + \varepsilon)d_{B0}\,, \tag{11}$$

where $\nu$ is the Poisson's ratio of the matrix. The initial tunneling distances of the two contacts ($d_{A0}$ and $d_{B0}$) can be determined through [16]

$$d_{A0} = d_{B0} = \alpha(c_1)^{\beta}\,, \tag{12}$$

where $\alpha$ and $\beta$ are calculated from

$$\begin{cases} d_m = \alpha(c_m)^{\beta} \\ d_p = \alpha(c_p)^{\beta} \end{cases}, \tag{13}$$

in which $c_p$ is the volume fraction of the graphene nanofillers at the percolation threshold of the sensor, $c_m$ is the highest possible volume fraction of the graphene nanofillers in the sensor, $d_p = 2t_{int}$, and $d_m = 0.34nm$ is the Van der Waals distance of graphene.

As shown in Figure 4, the contact area of a Type B contact is taken as half of the cross-sectional area of a coated graphene nanofillers, i.e.,

$$S_B = \frac{(b + 2t_{int})(t + 2t_{int})}{2}. \quad (14)$$

The contact area of a Type A contact highly depends on the states of the nanofillers and the interphase regions. For instance, an entangled graphene nanofiller would give rise to a smaller contact area than a stretched one.

The resistance of a nanocomposite sensor is linked to the tunneling resistances of the two types of contacts in the sensor by

$$R \propto fR_A + (1 - f)R_B\,, \quad (15)$$

where $f$ is the weighting factor of the Type A contacts in the sensor. The resistance change ratio of the sensor in responding to ultrasonic waves is defined by

$$\frac{\Delta R}{R_0} = \frac{R - R_0}{R_0}, \quad (16)$$

where $R_0$ is the initial resistance of the sensor in the absence of external strains.

By fitting Equation (16) to the resistance change ratios that are experimentally obtained at different strain levels, it is possible to approximate the contact area ($S_A$) and the weighting factor ($f$) in a sensor, enabling further analysis of the influence of the sizes of nanofillers and the properties of matrices on the ultrasonic sensing mechanism of thin-film graphene/polymer nanocomposite sensors.

### 3.4.Analysis of electrical conductivities of nanocomposite sensors based on experimental results and analytical model

The electrical conductivities of the two groups of nanocomposite sensors with various graphene contents were measured experimentally (see the Supplementary Information for the method).

As shown in Figure 5, the experimental measurements were fitted with the analytical model for the electrical conductivities of the sensors, i.e., Equation (7), to derive the thickness and the intrinsic electrical conductivity of the interphase regions in each sensor.

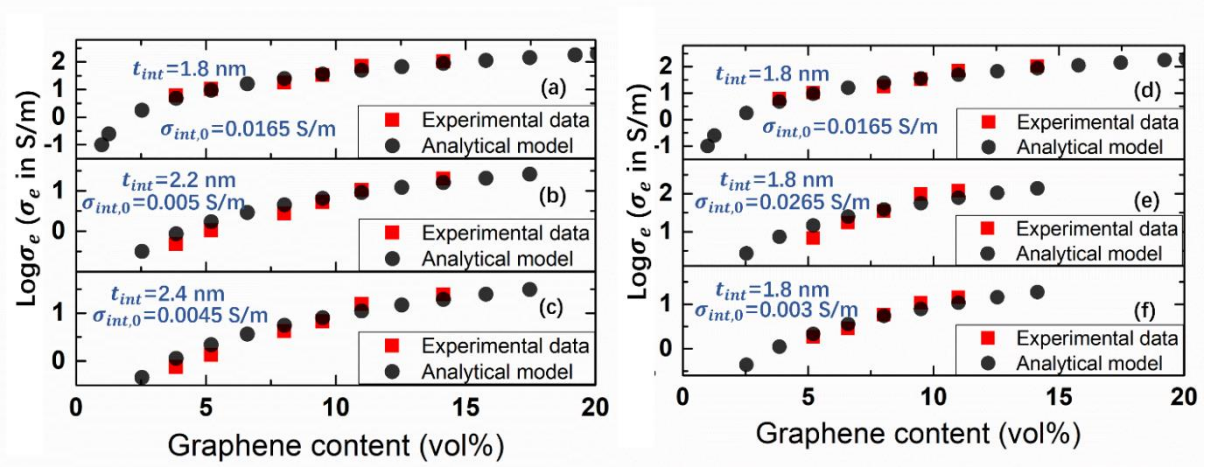


**Figure 5.** Experimentally measured electrical conductivities of nanocomposite sensors and their fittings with the analytical model: (a) G1, (b) G2, (c) G3, (d) M1, (e) M2 and (f) M3.

Based on Equation (6), the theoretical percolation thresholds of the Group 1 sensors were calculated to be 0.73 vol% (G1), 0.39 vol% (G2) and 0.78 vol% (G3) of graphene. G2 sensors, which are made from graphene nanofillers of the highest aspect ratio (diameter-to-thickness ratio), have the lowest percolation threshold. This finding is consistent with the trend reported in [13, 22], i.e., the percolation threshold of a graphene-based nanocomposite decreases as the aspect ratio of the graphene nanofillers used increases. It should be mentioned that in reality, it would be extremely difficult to fabricate thin-film nanocomposite sensors at their theoretical percolation thresholds using spray coating, because if a low graphene content is adopted, the nanofillers in the sensors fabricated would not be able to coalesce into conductive networks due to the sparseness of the spraying droplets and the relatively small number of spraying layers. Nevertheless, the experimental results shown in Figure 5 follow the trend depicted by the analytical model. Also, it is clear that the sensors with graphene contents between 5 and 10 vol%

retain the quantum tunneling effect.

The results in Figure 5(a)-(c) show that the sizes of graphene nanofillers greatly influence the thicknesses and the intrinsic electrical conductivities of interphase regions and, hence, the electrical conductivities of sensors. The difference between the electrical conductivities of the sensors with graphene nanofillers of the same diameter but different thicknesses, i.e., G1 and G2 sensors, is much larger than that in the case of the sensors with graphene nanofillers of different diameters but the same thickness, i.e., G2 and G3 sensors. This indicates that for a thin-film nanocomposite sensor, increasing the thickness of the graphene nanofillers has a more dominant effect, than increasing the diameter of the nanofillers, on increasing the electrical conductivity of the sensor. It is known that both the sizes of nanofillers and the thicknesses of interphase regions determine tunneling distances [26]. Therefore, G1 sensors, which contain interphase regions that are the thinnest, and graphene nanofillers that are both thick and large in diameter, would have the shortest tunneling distances between adjacent nanofillers, and consequently possess the highest electrical conductivities. Also, since the matrices of the three types of sensors are the same and, hence, have the same electrical conductivity, the difference between the intrinsic electrical conductivities of the interphase regions in these sensors could be related to a variation in the levels of entanglement of the graphene nanofillers in the sensors, influenced by the sizes of the nanofillers.

Sensors with different types of matrices also differ in electrical conductivity, as shown in Figure 5(d)-(f). The theoretical percolation thresholds of the three types of sensors were found to be the same, since the percolation threshold of a graphene-based nanocomposite is only

related to the size of the graphene nanofillers used [20, 27, 28], as depicted by Equation (6). It should be noted that for a CNT-based nanocomposite, the percolation threshold is also related to the properties of the matrix used [29]. Also due to the use of the same type of graphene nanofillers, the thicknesses of the interphase regions in the three types of sensors would be the same. Therefore, the finding that M1 and M2 sensors have much higher electrical conductivities than M3 sensors can be attributed to the higher electrical conductivities of their matrices, i.e., PVA and PVP, and the lower imperfection levels of their interphase regions, which would have led to the higher intrinsic electrical conductivities of the interphase regions.

For a sensor that is at or above its percolation threshold, i.e., when the tunneling paths inside the sensor are well established, the electrical conductivity of the sensor is related to the potential barrier height of the matrix used. Generally speaking, the larger the potential barrier height of the matrix is, the lower the electrical conductivity of the sensor would be [29]. The potential barrier heights of M1, M2 and M3 sensors will be presented in the next section, where the influence of the potential barrier heights on the electrical conductivities of the sensors will be discussed.

### 3.5.Analysis of sensitivities of nanocomposite sensors based on experimental results and analytical model

The resistance change ratios that would be exhibited by nanocomposite sensors with different weighting factors of Type A contacts, i.e., $f$, at different tensile strain levels were calculated using Equation (16) and are plotted in Figure 6(a). It can be seen that the sensitivities of the sensors, reflected by the gradients of the lines, i.e., the GFs, are highly dependent on $f$. Figure

6(b) illustrates the effects of both $f$ and the contact areas of Type A contacts, i.e., $S_A$, on sensitivities. The observation that under the same $S_A$, an increase in $f$ causes the sensitivity of a sensor to drop can explained by the fact that under a tensile strain, Type B contacts contribute positively to the sensitivity, while the effect of Type A contacts is the opposite. When $f$ is small, Type B contact mode is the dominant tunneling mechanism, resulting in high sensitivities. As $f$ increases, the dominant tunneling mechanism shifts to Type A contact mode, hence intensifying the influence of $S_A$ on sensitivities. A lower $S_A$ reflects that the graphene nanofillers in a sensor are more entangled and, consequently, Type A contacts contribute more significantly to the reduction of the sensitivity of the sensor.

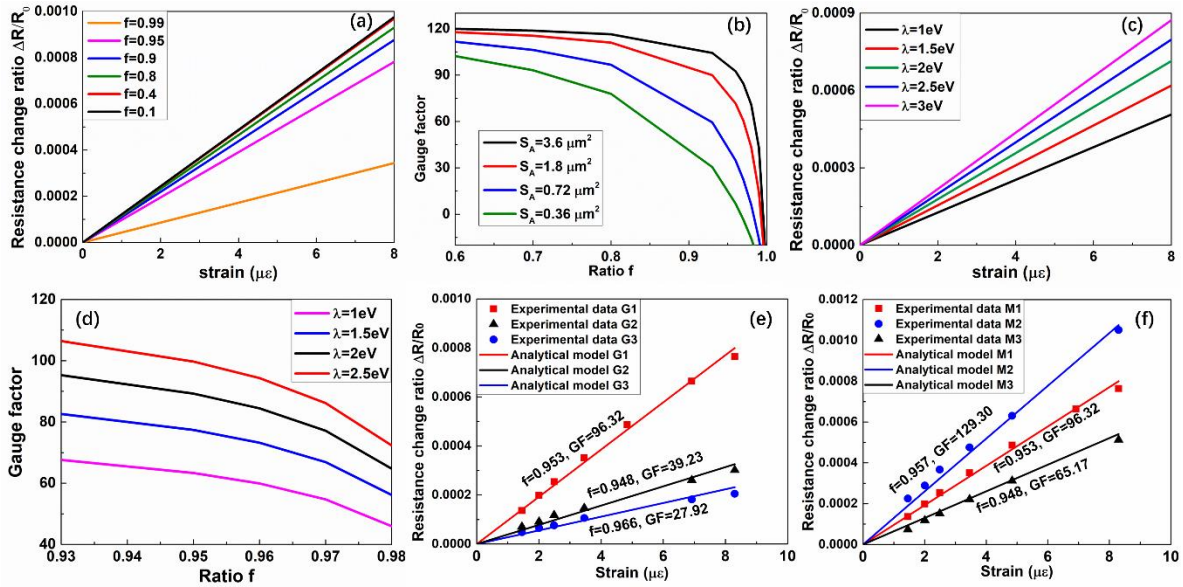


**Figure 6.** (a) Resistance change ratios of nanocomposite sensors with different weighting factors of Type A contacts ($f$) at different strains. (b) GFs of sensors with different Type A contact areas ($S_A$) at different $f$. (c) Resistance change ratios of sensors with different tunneling barrier heights ($\lambda$) at different strains. (d) GFs of sensors with different $\lambda$ at different $f$. Experimentally resistance change ratios of nanocomposite sensors (graphene content: 8.5 vol%) at various strains and their fittings with the analytical model: the $S_0$ modes received by (e) Group 1 sensors and (f) Group 2 sensors.

The resistance change ratios that would be exhibited by nanocomposite sensors with different tunneling barrier heights, i.e., $\lambda$, were also calculated, as shown in Figure 6(c). The

results indicate that sensitivities are also highly related to $\lambda$ with larger $\lambda$ leading to higher sensitivities. Figure 6(d) demonstrates that $\lambda$ could have more significant influence on sensitivities than $f$ does.

Excitation signals, each with a distinct peak voltage, were applied to the PZT wafer to induce ultrasonic waves. The peak amplitudes of the $S_0$ modes received by the nanocomposite sensors were extracted and then converted into electrical resistance changes based on the electrical properties of the bridge circuit / amplifier unit. Also, the peak strains experienced by the sensors under the different excitation voltages were calculated (see the Supplementary Information for the method). By plotting the resistance change ratios against the peak strains, the sensitivities of the sensors to the $S_0$ modes were evaluated. The experimental results were fitted with Equation (16), as shown in Figure 6(e) and (f). The thicknesses of the interphase regions in the sensors obtained in Section 3.4 were used in the analytical model to calculate tunneling resistances. It is worth mentioning that in order to ensure the validity of the analysis performed in this section, the repeatability of all the sensors used were ascertained as illustrated in the Supplementary Information.

Sensors with graphene nanofillers of different sizes possess different sensitivities, as demonstrated in Figure 6(e). Both the experimental results and the analytical modelling present linear relationships between resistance change ratios and ultrasonic wave-induced strains. $f$ of the three sensors are all close to 1, indicating that Type A contact mode is much more dominant than Type B contact mode. $S_A$ of the three sensors, derived from the model fitting, are 3.605 $\mu m^2$ (G1), 0.554 $\mu m^2$ (G2) and 0.301 $\mu m^2$ (G3). Comparing the two sensors with

graphene nanofillers of the same diameter, i.e., the G1 and the G2 sensor, the larger thickness of the nanofillers in the G1 sensor gave rise to a larger $S_A$, because the nanofillers in the sensor are less entangled as shown in Figure S6 in the Supplementary Information. Consequently, the G1 sensor possesses a higher sensitivity, as predicted in Figure 6(b). Although the G1 sensor has a larger $f$ than the G2 sensor, its significantly larger $S_A$ overwhelms the negative influence of $f$ on its sensitivity. Furthermore, the higher electrical conductivity of the G1 sensor (see Figure 5), which is related due to the larger thickness of its graphene nanofillers and the higher intrinsic electrical conductivity of its interphase regions, provides the basis for its superior sensitivity. Comparing the two sensors with graphene nanofillers of the same thickness, i.e., the G2 and the G3 sensors, the smaller diameter of the nanofillers in the G3 sensor understandably resulted in a smaller $S_A$, causing the G3 sensor to possess a lower sensitivity, though the nanofillers in the G3 sensor also exhibit a low level of entanglement, as shown in Figure S6, due to their low aspect ratio.

Figure 6(f) shows the sensitivities of nanocomposite sensors with different types of matrices. The relationships between electrical resistance changes and ultrasonic wave-induced strains also follow linear trends. $S_A$ of the three sensors were found, through the model fitting, to be 3.605 $\mu m^2$ (M1), 18.022 $\mu m^2$ (M2) and 1.802 $\mu m^2$ (M3). Since the graphene nanofillers in the three sensors are of the same size and, hence, would have exhibited the same level of entanglement, the difference in $S_A$ can be attributed to a variation in the imperfection levels of the interphase regions in these sensors, caused by the use of different types of matrix materials. More specifically, a larger $S_A$ is the result of interphase regions with a lower

imperfection level. Also through the model fitting, the tunneling barrier heights of the three sensors were found to be 2.4 eV (M1), 2.8 eV (M2) and 1.5 eV (M3), reasonable compared with the values reported in [16, 18]. The M2 sensor, which has the largest tunneling barrier height and contains interphase regions with the lowest imperfection level, as reflected by the intrinsic electrical conductivity of its interphase regions (see Figure 5), possesses the highest sensitivity.

It is interesting to note that the M2 sensor, which has the largest tunneling barrier height, actually exhibits the highest electrical conductivity (see Figure 5), a finding that is inconsistent with [29]. This could be attributed to the fact that the electrical conductivity of a sensor increases as the imperfection level of the interphase regions in the sensor decreases [14]. For the three sensors concerned, the imperfection levels of interphase regions might have been more dominant than the tunneling barrier heights of matrices in determining the electrical conductivity of a sensor. Therefore, the M2 sensor, which has the largest tunneling barrier height but contains interphase regions with the lowest imperfection level, exhibits the highest electrical conductivity.

The sensitivities of the nanocomposite sensors to the $A_0$ modes are presented in the Supplementary Information. From the results obtained in this section, it can be concluded that in acquiring ultrasonic waves, the sensitivity of a thin-film graphene/polymer nanocomposite sensor is positively related to the thickness and the diameter of the nanofillers. Furthermore, matrices that have large tunneling barrier heights and result in interphase regions with low imperfection levels also contribute to improving sensitivities. The findings that have been

obtained in this work on the electrical conductivities and the ultrasonic sensitivities of thin-film graphene/polymer nanocomposite sensors are summarized in Figure 7.

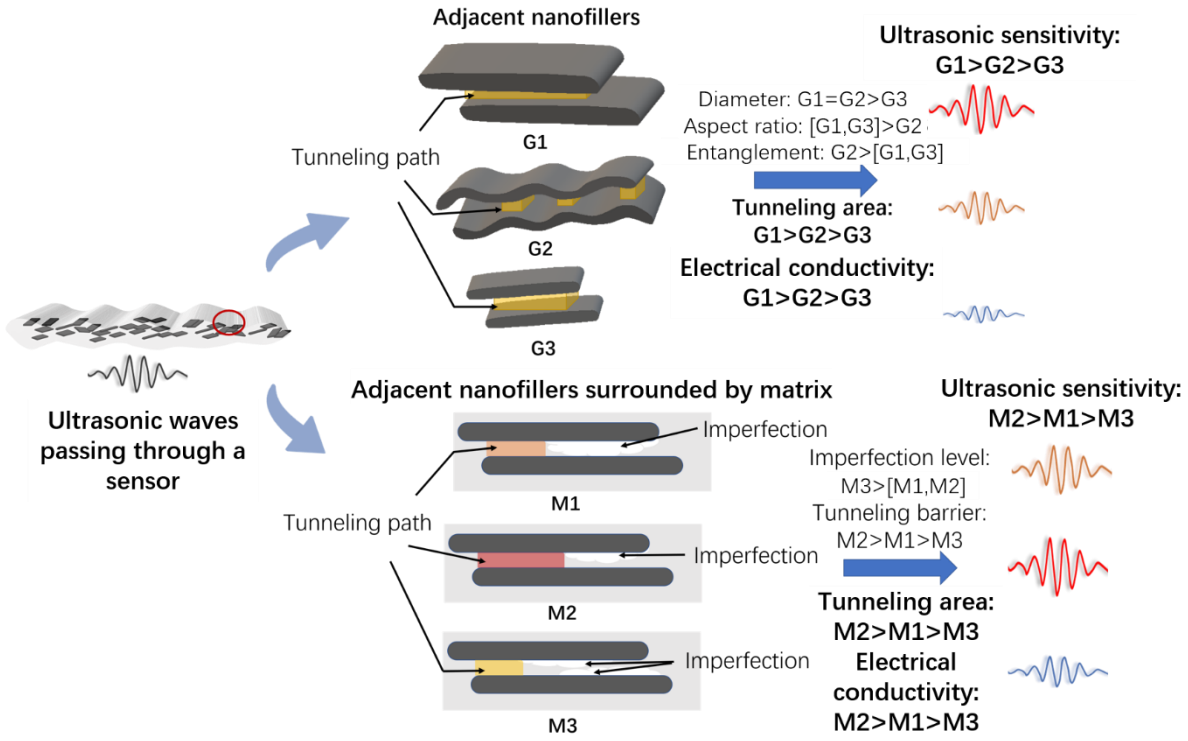


**Figure 7.** Summary of the effects of the properties of nanofillers and matrices on the microstructures, the electrical conductivities, and the ultrasonic sensitivities of thin-film graphene/polymer nanocomposite sensors.

## 4. Conclusion

The ultrasonic sensing mechanism of thin-film graphene/polymer nanocomposite strain sensors has been evaluated through complimentary physical experiments and analytical modeling. At first, it was observed, through ultrasonic sensing experiments, that the sensitivity of a sensor is significantly influenced by the size of the graphene nanofillers and the type of the matrix. Analytical models that entail interphase regions and the quantum tunneling effect were then established and fitted to the experimental results with a view to understand the underlying reasons of the experimental observations. Through an in-depth analysis, it was revealed that the sizes of graphene nanofillers and the properties of matrix materials,

collectively or separately, determine the thicknesses, the imperfection levels and the electrical conductivities of interphase regions, the contact areas between adjacent nanofillers, and the electrical conductivities and the tunneling barrier heights of matrices. These parameters, in turn, dictate the electrical conductivities and the ultrasonic sensitivities of nanocomposite sensors. This study presents a constructive starting point for enabling precision manufacturing of thin-film graphene/polymer nanocomposite strain sensors used for acquiring ultrasonic waves, driving these sensors one step closer to realizing their intended application of *in situ* structural integrity monitoring.

## References


1. Li, Y.H., Y.Z. Liao, and Z.Q. Su, *Graphene-functionalized polymer composites for self-sensing of ultrasonic waves: An initiative towards "sensor-free" structural health monitoring.* Composites Science and Technology, 2018. **168**: p. 203-213.
2. Duan, F., Y.Z. Liao, Z.H. Zeng, H. Jin, L.M. Zhou, Z. Zhang, and Z.Q. Su, *Graphene-based nanocomposite strain sensor response to ultrasonic guided waves.* Composites Science and Technology, 2019. **174**: p. 42-49.
3. Liao, Y.Z., F. Duan, H.T. Zhang, Y. Lu, Z.H. Zeng, M.L. Liu, H. Xu, C. Gao, L.M. Zhou, H. Jin, Z. Zhang, and Z.Q. Su, *Ultrafast response of spray-on nanocomposite piezoresistive sensors to broadband ultrasound.* Carbon, 2019. **143**: p. 743-751.
4. Stauffer, D. and A. Aharony, *Introduction to percolation theory*. 2018: CRC press.
5. Chang, L., K. Friedrich, L. Ye, and P. Toro, *Evaluation and visualization of the percolating networks in multi-wall carbon nanotube/epoxy composites.* Journal of Materials Science, 2009. **44**(15): p. 4003-4012.
6. Kara, S., E. Arda, F. Dolastir, and O. Pekcan, *Electrical and optical percolations of polystyrene latex-multiwalled carbon nanotube composites.* J Colloid Interface Sci, 2010. **344**(2): p. 395-401.
7. Mazaheri, M., J. Payandehpeyman, and M. Khamehchi, *A developed theoretical model for effective electrical conductivity and percolation behavior of polymer-graphene nanocomposites with various exfoliated filleted nanoplatelets.* Carbon, 2020. **169**: p. 264-275.
8. Bhuiyan, M.Z.A., G. Wang, J. Cao, and J. Wu, *Deploying wireless sensor networks with fault-tolerance for structural health monitoring.* IEEE Transactions on Computers, 2015. **64**(2): p. 382-395.
9. Zheng, Y.J., Y.L. Li, Z.Y. Li, Y.L. Wang, K. Dai, G.Q. Zheng, C.T. Liu, and C.Y. Shen, *The effect of filler dimensionality on the electromechanical performance of polydimethylsiloxane based conductive nanocomposites for flexible strain sensors.* Composites Science and Technology, 2017. **139**: p. 64-73.
10. Zhao, J., C.L. He, R. Yang, Z.W. Shi, M. Cheng, W. Yang, G.B. Xie, D.M. Wang, D.X. Shi, and G.Y. Zhang, *Ultra-sensitive strain sensors based on piezoresistive nanographene films.* Applied Physics Letters, 2012. **101**(6): p. 063112.
11. Zhao, J., G. Wang, R. Yang, X. Lu, M. Cheng, C. He, G. Xie, J. Meng, D. Shi, and G. Zhang, *Tunable piezoresistivity of nanographene films for strain sensing.* ACS Nano, 2015. **9**(2): p. 1622-9.

12. Taherian, R., *Experimental and analytical model for the electrical conductivity of polymer-based nanocomposites.* Composites Science and Technology, 2016. **123**: p. 17-31.
13. Hashemi, R. and G.J. Weng, *A theoretical treatment of graphene nanocomposites with percolation threshold, tunneling-assisted conductivity and microcapacitor effect in AC and DC electrical settings.* Carbon, 2016. **96**: p. 474-490.
14. Xia, X., J. Hao, Y. Wang, Z. Zhong, and G.J. Weng, *Theory of electrical conductivity and dielectric permittivity of highly aligned graphene-based nanocomposites.* J Phys Condens Matter, 2017. **29**(20): p. 205702.
15. Sánchez, M., R. Moriche, X.F. Sánchez-Romate, S.G. Prolongo, J. Rams, and A. Ureña, *Effect of graphene nanoplatelets thickness on strain sensitivity of nanocomposites: A deeper theoretical to experimental analysis.* Composites Science and Technology, 2019. **181**: p. 107697.
16. Kuronuma, Y., T. Takeda, Y. Shindo, F. Narita, and Z.J. Wei, *Electrical resistance-based strain sensing in carbon nanotube/polymer composites under tension: Analytical modeling and experiments.* Composites Science and Technology, 2012. **72**(14): p. 1678-1682.
17. Bao, W.S., S.A. Meguid, Z.H. Zhu, and G.J. Weng, *Tunneling resistance and its effect on the electrical conductivity of carbon nanotube nanocomposites.* Journal of Applied Physics, 2012. **111**(9): p. 093726.
18. Hu, N., Y. Karube, C. Yan, Z. Masuda, and H. Fukunaga, *Tunneling effect in a polymer/carbon nanotube nanocomposite strain sensor.* Acta Materialia, 2008. **56**(13): p. 2929-2936.
19. Guan, R., F. Zou, Z. Weng, P. Zhou, Y. Liao, Z. Su, and L. Huang, *On a Highly Reproducible, Broadband Nanocomposite Ultrasonic Film Sensor Fabricated by Ultrasonic Atomization-Assisted Spray Coating.* Advanced Engineering Materials, 2020. **22**(11): p. 2000462.
20. Payandehpeyman, J., M. Mazaheri, and M. Khamehchi, *Prediction of electrical conductivity of polymer-graphene nanocomposites by developing an analytical model considering interphase, tunneling and geometry effects.* Composites Communications, 2020. **21**: p. 100364.
21. Wang, Y., G.J. Weng, S.A. Meguid, and A.M. Hamouda, *A continuum model with a percolation threshold and tunneling-assisted interfacial conductivity for carbon nanotube-based nanocomposites.* Journal of Applied Physics, 2014. **115**(19): p. 193706.
22. Li, J. and J.K. Kim, *Percolation threshold of conducting polymer composites containing 3D randomly distributed graphite nanoplatelets.* Composites Science and Technology, 2007. **67**(10): p. 2114-2120.
23. Landau, L.D., J. Bell, M. Kearsley, L. Pitaevskii, E. Lifshitz, and J. Sykes, *Electrodynamics of continuous media*. Vol. 8. 2013: Elsevier.
24. Eshelby, J.D., *The determination of the elastic field of an ellipsoidal inclusion, and related problems.* Proceedings of the royal society of London. Series A. Mathematical and physical sciences, 1957. **241**(1226): p. 376-396.
25. Weng, G.J., *A dynamical theory for the Mori-Tanaka and Ponte Castaneda-Willis estimates.* Mechanics of Materials, 2010. **42**(9): p. 886-893.
26. Zare, Y. and K.Y. Rhee, *Calculation of tunneling distance in carbon nanotubes nanocomposites: effect of carbon nanotube properties, interphase and networks.* Journal of Materials Science, 2020. **55**(13): p. 5471-5480.
27. Lu, X., J. Yvonnet, F. Detrez, and J. Bai, *Multiscale modeling of nonlinear electric conductivity in graphene-reinforced nanocomposites taking into account tunnelling effect.* Journal of Computational Physics, 2017. **337**: p. 116-131.
28. Manta, A., M. Gresil, and C. Soutis, *Predictive model of graphene based polymer nanocomposites: electrical performance.* Applied Composite Materials, 2017. **24**(2): p. 281-300.
29. Fang, C., J. Zhang, X. Chen, and G. Weng, *Calculating the Electrical Conductivity of Graphene Nanoplatelet Polymer Composites by a Monte Carlo Method.* Nanomaterials, 2020. **10**: p. 1129.